IUST Iran University of Science and Technology

Iranian Journal of Electrical and Electronic Engineering

Journal Homepage: ijeee.iust.ac.ir

Research Paper

Discrete Time Control Method for SVM Direct Active Power and Stator Flux Control of PMSG-Based Wind Turbine

B. Mamipour Matanag*, N. Rostami*(C.A.), and S. Tohidi*

Abstract: This paper proposes a new method for direct control of active power and stator flux of permanent magnet synchronous generator (PMSG) used in the wind power generation system. Active power and stator flux are controlled by the proposed discrete time algorithm. Despite the commonly used vector control methods, there is no need for inner current control loops. To decrease the errors between reference and measured values of active power and stator flux, the space vector modulation (SVM) is used, which results in a constant switching frequency. Compared to vector control, the proposed direct control method has advantages such as higher dynamic response due to elimination of inner current control loops and no need to coordinate system transformation blocks as well as the PI controllers and their adjustment. Moreover, permanent magnet flux vector and several machine parameters such as stator inductances are not required which can improve the robustness of the control system. The proposed method can be used in both types of surface-mounted and interior PMSGs. The effectiveness of the proposed method in comparison to the vector control method with optimized PI coefficients by the particle swarm algorithm is evaluated. Simulation results performed in MATLAB/Simulink software show that higher dynamic response with lower active power and the stator flux ripple are achieved with the proposed method.

Keywords: Direct Power Control (DPC), Vector Control, Permanent Magnet Synchronous Generator (PMSG), Wind Power Generation System.

1 Introduction

DRAMATIC increase in the demand for electric energy, reduction of the natural resources, and increase of the environmental concerns have led to more attention to renewable energies including wind turbines. Considering the benefits of renewable energy generations, it is expected that they will have a major role in future power grids.

Specific features of permanent magnet synchronous generators (PMSG) such as high torque density, desirable power density, desirable efficiency, make them an appropriate generator for wind turbines.

Iranian Journal of Electrical and Electronic Engineering, 2021.
Paper first received 30 November 2019, revised 20 July 2020, and accepted 27 July 2020.
* The authors are with the Faculty of Electrical and Computer Engineering, University of Tabriz, Tabriz, Iran.
E-mails: bmamipour964@gmail.com, an-rostami@tabrizu.ac.ir, and stohidi@tabrizu.ac.ir.
Corresponding Author: N. Rostami.
https://doi.org/10.22068/IJEEE.17.2.1720

Different control techniques have been used for PMSG. Vector control is one of the most popular drive methods due to advantages such as desirable steady-state response, low torque ripple, and low switching frequency [1]. However, it suffers from some challenges which affect the transient response. To maintain the system stability and to achieve a better dynamic response, it is necessary to adjust the proportional integral (PI) controller coefficients properly [2-4]. This method also has a high sensitivity to the machine parameter's variations, and accurate estimation of the rotor position is required for coordinate transformations [5].

To overcome the aforementioned problems, switching table based DTC/DPC methods have been presented [6]. The core idea of such methods is direct control of the torque/power without controlling the stator current by using a predefined switching table. However, the performance of DTC depends on the hysteresis band and the predefined switching table. This system has drawbacks such as variable switching frequency, and high torque and flux ripple [7-10]. Therefore, some improved DTC schemes such as SVM-DTC, and the model predictive direct torque/power control have been proposed.

SVM-DTC has been proposed to achieve the advantages of both the vector and direct control such as constant switching frequency and reliable low-speed operation and, at the same time, accurate control of torque and flux. In [11, 12], SVM-DTC method based on flux oriented control has been used. Even though, a constant switching frequency is achieved the dynamic response of the system is lowered. The coordinate transformation block is not required for the proposed method in [13] and the electromagnetic torque is directly controlled via the load angle. The proposed control method is capable of decreasing the torque ripple of PMSG. However, it needs information of the machine parameters, including the stator inductance and PM flux. Besides, the optimal adjustment of the PI coefficients is a challenging task.

In deadbeat control, the optimum reference voltage vector is determined by predicting the current trajectory. In [14], deadbeat control has been implemented to compensate the torque and flux errors in SVM-DTC. The problem however is that this method is highly dependent on the machine parameters and inaccurate modeling of the machine may lead to significant error.

In recent years, model predictive control has been attracted more attention in high performance drive systems [15-19]. In this method, a flexible cost function with different control purposes is used to produce the proper voltage vectors instead of a predefined switching table and hysteresis band. It must be noted that the switching frequency should be limited in an acceptable range. Even though, the steady-state response can be improved with higher switching frequencies. However, the switching losses and hardware costs will be increased [15, 16].

In [17, 18], a direct model predictive power control (DMPPC) has been presented to enhance the steady-state response of the system. In [18], the steady-state response of the surface-mounted PM synchronous machine has been improved by optimization of the duty cycle by using DMPPC method. In the proposed method an extra zero vector has been used to minimize the cost function. However, the equivalent voltage vector phase is still limited to active vectors. In [19], a new method based on DMPPC has been presented to reduce the power ripple by selecting a non-zero voltage vector in a fraction of control period and allocation of a zero vector in the rest of time. However, the effectiveness of the method highly depends on the machine model accuracy. Furthermore, heavy computations are required for MPC, increases the hardware cost.

This paper proposes a new discrete time control method for direct active power and stator flux control of interior permanent magnet synchronous generator. The novelty of the proposed method is utilizing the discrete time algorithm in SVM-DPC method, where a reference voltage vector is defined using the desired stator flux vector. The desired stator flux itself is predicted for the next time interval by using only active power and stator flux information. In the proposed discrete control method, the controlling principal is obtained in the view of the flux space vector and load angle. The proposed method is less sensitive to the machine parameters such as stator inductance and PM flux vector improving dynamic response.

The switching frequency is stabilized by using SVM and, dynamic response is enhanced due to the absence of inner current control loops. All the calculations are carried out only in the stationary reference frame. Another advantage of the proposed method is elimination of PI controllers. The proposed method can be used in both types of surface-mounted PMSG (SPMSG) and interior PMSG (IPMSG).

A comparison between the results obtained for the proposed method and conventional vector control with optimum PI coefficient optimized by particle swarm optimization algorithm validates the effectiveness of the proposed method. Higher dynamic response and lower active power and stator flux ripple are achieved by the proposed method. MATLAB/Simulink is used for simulation.

2 Direct Drive Wind Turbine with PMSG

The structure of the wind turbine with PMSG is depicted in Fig. 1, where the wind turbine is directly connected to the PMSG. A machine side converter (MSC) and a grid-side converter (GSC) are connected back to back through a DC link and transmit the electrical power generated by PMSG to the power grid. In this paper, a standard two levels fully controlled power converter is used.

2.1 Wind Turbine and Shaft Aerodynamic Model

The mechanical power extracted by the wind turbine from the wind is expressed as the following equation:

$$P_m = \frac{1}{2}\rho\pi R^2 V^3 C_p(\lambda,\theta) \tag{1}$$

where R, ρ, and V are the blade radius (m), the air density (kg/m^3), and wind speed (m/s) respectively. C_p is the power coefficient which is related to the pitch angle θ (deg) and tip-speed ratio λ which is defined as:

$$\lambda = \frac{\omega_t R}{V} \tag{2}$$

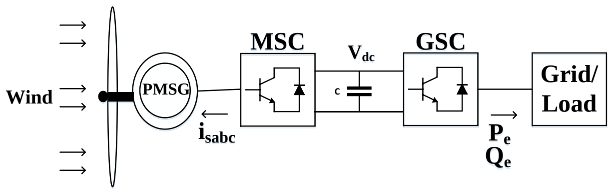

Fig. 1 Direct drive wind turbine with PMSG.

where ω_t is the turbine shaft speed (rad/s). According to [13], C_p is defined as:

$$C_p = \frac{1}{2}\left(\lambda - 1.616\right)\exp\left(-0.2542.\lambda\right) \tag{3}$$

C_p should be maximized to obtain the maximum power point tracking (MPPT). According to (3), the maximum power coefficient $C_{p\text{-max}}$ is 0.48 for the optimum value of tip-speed ratio λ_{opt} = 5.55. The turbine shaft speed should be adjusted to optimal value $\omega_{t\text{-}opt}$ to maximize the power extraction from the wind.

$$\omega_{t\text{-}opt} = \frac{\lambda_{opt}}{R} v \tag{4}$$

Therefore, the maximum power P_{opt} that can be extracted from the wind is expressed as:

$$P_{opt} = K_{opt}\,\omega_{t\text{-}opt}^3 \tag{5}$$

$$K_{opt} = \frac{1}{2}\rho\pi R^5 \frac{C_{p\text{-max}}}{\lambda_{opt}^3} \tag{6}$$

where K_{opt} is the constant coefficient which is determined by the turbine characteristics.

PMSG is directly connected to the wind turbine. Therefore, the dynamic motion equation is [13]:

$$2H\frac{d\omega_t}{dt} = \frac{P_m}{\omega_t} - \frac{P_e}{\omega_t} - D\omega_t \tag{7}$$

where $2H$ is the total inertia constant of turbine and PMSG ($kg.m^2$), P_e is the air gap or electromagnetic power (W) produced by the PMSG, P_m is the mechanical input power, and D is the damping coefficient ($kg.m^2/s$).

2.2 PMSG Model

The dynamic model of a three-phase PMSG in the synchronously rotating dq reference frame is expressed as:

$$\frac{d}{dt}\psi_{sd} = V_{sd} - R_s i_{sd} + \omega_e \psi_{sq} \tag{8}$$

$$\frac{d}{dt}\psi_{sq} = V_{sq} - R_s i_{sq} + \omega_e \psi_{sd} \tag{9}$$

where V_{sd} and V_{sq} are the stator voltages in the d and q axis, respectively; i_{sd} and i_{sq} are the stator currents in the d and q axis, respectively; R_s is the stator winding resistance and $\omega_e$is the rotor electrical angular speed. ψ_{sd}, ψ_{sq} are the stator flux linkage of the machine in the d and q axis, respectively, and are defined as:

$$\psi_{sd} = L_d i_{sd} + \psi_m \tag{10}$$

$$\psi_{sq} = L_q i_{sq} \tag{11}$$

where L_d and L_q are the d and q axis inductances of the machine, respectively. ψ_m is the flux linkage produced by the PMs. The machine electromagnetic torque is:

$$T_e = \frac{3p}{2}\psi_m i_{sq} + \frac{3p}{2}(L_d - L_q) i_{sd} i_{sq} \tag{12}$$

where p is the number of pole pairs. T_e can also be expressed as a function of the load angle δ and the magnitude of stator flux linkage ($|\psi_s|$) [13].

$$T_e = \frac{3}{2}\frac{p}{L_d}|\psi_s|\psi_m \sin\delta + \frac{3}{4}\frac{p}{L_d L_q}|\psi_s|^2\left(L_d - L_q\right)\sin\left(2\delta\right) \tag{13}$$

According to (12) and (13), the electromagnetic torque has two terms. The first term is related to the magnetic torque, and the second nonlinear term corresponds to the reluctance torque produced due to the machine saliency. Compared to the surface-mounted PMSGs ($L_d = L_q$), higher level of torque can be produced by interior PMSGs ($L_d \neq L_q$) with the same level of d-q axis stator currents. However, the mathematical equation of T_e becomes more complicated. In [20, 21], the concept of active flux has been introduced to combine the two aforementioned terms as one single term. By using this concept, an interior PMSG can be analyzed like a surface-mounted PMSG. The active flux magnitude $\left|\psi_d^\alpha\right|$ is defined as [20]:

$$\left|\psi_d^\alpha\right| = \psi_m + \left(L_d - L_q\right) i_{sd} \tag{14}$$

By substituting i_{sq} from (11) into (12), T_e can be expressed as (13) and the active flux concept can be implemented.

$$T_e = \frac{3p}{2}\left[\psi_m + \left(L_d - L_q\right) i_{sd}\right]\frac{\psi_{sq}}{L_q} \tag{15}$$

Since $\psi_{sq} = |\psi_s|\sin\delta$, (15) can be rewritten in terms of the active flux magnitude, stator flux magnitude, and load angle as:

$$T_e = \frac{3}{2}\frac{p}{L_q}|\psi_s|\left|\psi_d^\alpha\right|\sin\delta \tag{16}$$

The magnitude of active flux is calculated as a function of stator flux magnitude and load angle by dividing (13) by (16):

$$\left|\psi_d^\alpha\right| = \frac{L_q}{L_d}\left[\psi_m + \frac{|\psi_s|}{L_q}\left(L_d - L_q\right)\cos\delta\right] \tag{17}$$

3 Proposed Active Power and Stator Flux Control Method

This section proposes a new discrete-time method for direct active power and stator flux control of PMSG. The main idea of this method is the discrete control of the active power and stator flux, from the perspective of the flux space vector and angular load vector. The relationship between the flux and current vectors of PMSG is shown in the space vector diagram of Fig. 2, where $\psi_{s\alpha\beta}$, ψ_d^α, and $\psi_{m\alpha\beta}$ are the stator flux, active flux, and PM flux vectors, respectively. $i_{s\alpha\beta}$ is the stator current vector. θ_s, δ, and θ_{re} are the stator flux angle, load angle, and electrical rotor position, respectively. All the calculations are performed in the stationary reference frame.

Electromagnetic torque T_e and reactive torque T_r are defined as [22]:

$$T_e = \frac{3p}{2}\mathrm{Im}\left(\psi_{s\alpha\beta}^{*} i_{s\alpha\beta}\right) \tag{18}$$

$$T_r = \frac{3p}{2}\mathrm{Im}\left(j\,\psi_{s\alpha\beta} i_{s\alpha\beta}^{*}\right) \tag{19}$$

where “Im” indicates the imaginary part and the asterisk indicates the complex conjugate. In the above equations, $j = \sqrt{-1}$.

According to Fig. 2, the active flux vector ψ_d^α is aligned on the d-axis and is expressed as:

$$\psi_d^\alpha = \psi_{s\alpha\beta} - L_q i_{s\alpha\beta} \tag{20}$$

By substituting $i_{s\alpha\beta}$ from (20) in (19) and using $\theta_{re} = \delta + \theta_s$, according to Fig. 2, the reactive torque is expressed as:

$$T_r = \frac{3p}{2}\mathrm{Im}\left[j\,\frac{|\psi_s|\angle\theta_s}{L_q}\left(|\psi_s|\angle(-\theta_s) - |\psi_d^\alpha|\angle(-\theta_s-\delta)\right)\right] \tag{21}$$

Multiplying $|\psi_s|\angle\theta_s$ in the phrase inside the parenthesis yields:

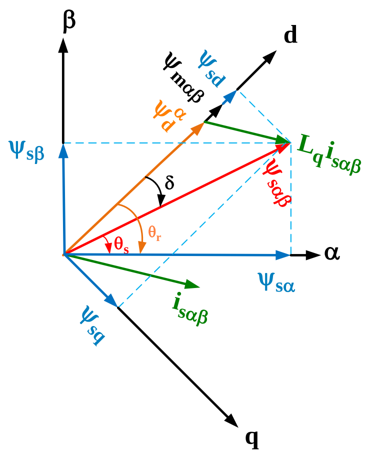

Fig. 2 Direct drive wind turbine with PMSG.

$$T_r = \frac{3p}{2}\mathrm{Im}\left[j\,\frac{1}{L_q}\left(|\psi_s|^2 - |\psi_s||\psi_d^\alpha|\angle(-\delta)\right)\right] \tag{22}$$

By using a polar-to-rectangular conversion, the real and imaginary parts of the phrase inside the parenthesis are obtained.

$$T_r = \frac{3p}{2}\mathrm{Im}\left[\frac{j}{L_q}\left(|\psi_s|^2 - |\psi_s||\psi_d^\alpha|\cos\delta + j\,|\psi_s||\psi_d^\alpha|\sin\delta\right)\right] \tag{23}$$

Then, multiplying j in the phrase inside the parenthesis gives:

$$T_r = \frac{3p}{2}\mathrm{Im}\left[\frac{1}{L_q}\left(j\,|\psi_s|^2 - j\,|\psi_s||\psi_d^\alpha|\cos\delta - |\psi_s||\psi_d^\alpha|\sin\delta\right)\right] \tag{24}$$

Finally, the reactive torque is defined by selecting the imaginary part of (24), as:

$$T_r = \frac{3p}{2L_q}\left(|\psi_s|^2 - |\psi_s||\psi_d^\alpha|\cos\delta\right) \tag{25}$$

If $|\psi_s||\psi_d^\alpha|$ from (16) is substituted in (25), the reactive torque is stated in terms of stator flux magnitude and electromagnetic torque as:

$$T_r = \frac{3p}{2L_q}|\psi_s|^2 - \frac{T_e}{\tan\delta} \tag{26}$$

$|\psi_s|^2$ is derived as:

$$|\psi_s|^2 = \frac{2L_q}{3p}\left(T_r + \frac{T_e}{\tan\delta}\right) \tag{27}$$

By multiplication of both sides of (27) in the electrical rotating speed ω_e, the active torque T_e is converted to active power P_e, and reactive torque T_r is converted to reactive power Q. With some computations effort, the following equation is obtained, which relates the active power to reactive power:

$$\frac{3p}{2L_q}\omega_e|\psi_s|^2 = Q + P_e\cot\delta \tag{28}$$

The derivative of both sides of (28) with respect to time yields:

$$\frac{3p}{2L_q}\left(|\psi_s|^2\frac{d\omega_e}{dt} + 2\omega_e|\psi_s|\frac{d|\psi_s|}{dt}\right) = \frac{dQ}{dt} + \cot\delta\frac{dP_e}{dt} - \left(1+\cot^2\delta\right)P_e\frac{d\delta}{dt} \tag{29}$$

In the k-th control step, (29) is written in the discrete-time domain as:

$$\frac{3p}{2L_q}\left(\left|\psi_s[k]\right|^2\Delta\omega_e[k]+2\omega_e[k]\left|\psi_s[k]\right|\Delta\left|\psi_s[k]\right|\right)=$$
$$\Delta Q[k]+\Delta P_e[k]\cot\delta[k]-\left(1+\cot^2\delta[k]\right)P_e[k]\Delta\delta[k] \quad (30)$$

Equation (28) can also be expressed in the discrete time domain as follows:

$$\frac{3p}{2L_q}\omega_e[k]\left|\psi_s[k]\right|^2=Q[k]+P_e[k]\cot\delta[k] \quad (31)$$

dividing (30) by (31) yields:

$$\frac{\Delta\omega_e}{\omega_e[k]}+2\frac{\Delta\left|\psi_s[k]\right|}{\left|\psi_s[k]\right|}=$$
$$\frac{\Delta Q[k]+\Delta P_e[k]\cot\delta[k]}{Q[k]+P_e[k]\cot\delta[k]}$$
$$-\frac{\left(1+\cot^2\delta[k]\right)P_e[k]\Delta\delta[k]}{Q[k]+P_e[k]\cot\delta[k]} \quad (32)$$

Euler approximation method is taken into account in this paper. In this method, the derivative of a variable in a distinctive interval in the discrete-time domain, with the Δ operator, is approximated by the difference between the values of the variable at the current and next moment. Since the purpose of the controller is to get the variable closer to its reference value at the next moment, the value of the variable at the next moment is considered as the reference value. The errors of active power, reactive power, stator flux magnitude, and electrical rotating speed are calculated by using their corresponding reference and estimated values, as:

$$\Delta P_e[k]=P_e^*[k]-P_e[k] \quad (33)$$
$$\Delta Q[k]=Q^*[k]-Q[k] \quad (34)$$
$$\Delta\left|\psi_s[k]\right|=\left|\psi_s[k]\right|^*-\left|\psi_s[k]\right| \quad (35)$$
$$\Delta\omega_e[k]=\omega_e^*[k]-\omega_e[k] \quad (36)$$

where asterisk superscripts indicate the reference values.

Substituting by (33-36) into (32) gives:

$$\frac{\omega_e^*[k]-\omega_e[k]}{\omega_e[k]}+2\frac{\left|\psi_s[k]\right|^*-\left|\psi_s[k]\right|}{\left|\psi_s[k]\right|}=$$
$$\frac{Q^*[k]-Q[k]+\left(P_e^*[k]-P_e[k]\right)\cot\delta[k]}{Q[k]+P_e[k]\cot\delta[k]}$$
$$-\frac{\left(1+\cot^2\delta[k]\right)P_e[k]\Delta\delta[k]}{Q[k]+P_e[k]\cot\delta[k]} \quad (37)$$

Equation (37) is simplified as:

$$\frac{\omega_e^*[k]}{\omega_e[k]}+2\frac{\left|\psi_s[k]\right|^*}{\left|\psi_s[k]\right|}-2=\frac{Q^*[k]+P_e^*[k]\cot\delta[k]}{Q[k]+P_e[k]\cot\delta[k]}$$
$$-\frac{P_e[k]\Delta\delta[k]\left(1+\cot^2\delta[k]\right)}{Q[k]+P_e[k]\cot\delta[k]} \quad (38)$$

From (38), the increment of load angle $\Delta\delta[k]$ is derived as:

$$\Delta\delta[k]=$$
$$\frac{Q[k]+P_e[k]\cot\delta}{P_e[k]\left(1+\cot^2\delta[k]\right)}\times\left(\frac{Q^*[k]+P_e^*[k]\cot\delta[k]}{Q[k]+P_e[k]\cot\delta[k]}\right.$$
$$\left.-\frac{\omega_e^*[k]}{\omega_e[k]}-2\frac{\left|\psi_s[k]\right|^*}{\left|\psi_s[k]\right|}+2\right) \quad (39)$$

To realize MPPT, the optimal active power is proportional to the cube of rotating speed (according to (5)). Therefore, the electrical rotating speed is expressed in terms of active power. Equation (39) can then be written as:

$$\Delta\delta[k]=$$
$$\frac{Q[k]+P_e[k]\cot\delta[k]}{P_e[k]\left(1+\cot^2\delta[k]\right)}\times\left(\frac{Q^*[k]+P_e^*[k]\cot\delta[k]}{Q[k]+P_e[k]\cot\delta[k]}\right.$$
$$\left.-\sqrt[3]{\frac{P_e^*[k]}{P_e[k]}}-2\frac{\left|\psi_s[k]\right|^*}{\left|\psi_s[k]\right|}+2\right) \quad (40)$$

where P and ψ are the variables that are being controlled.

As evident from (40), the obtained control law less depends on the machine parameters such as stator inductances and PM flux linkage. Since the accurate estimation of the machine parameters is a sophisticated task [23, 24], this can be considered as the main advantage of the proposed method.

In this paper, the aim is to control the active power and stator flux, and it is assumed that the reference power factor is equal to one. So, in (40), $Q^*[k]$ will be zero.

The reference flux angle $\theta_s^*[k]$ is achieved from the following equation:

$$\theta_s^*[k]=\Delta\delta[k]+\theta_s[k] \quad (41)$$

In accordance with (41) and with the desired magnitude of stator linkage $|\psi_s[k]|^*$, the reference of the stator flux in the stationary reference frame is stated as:

$$\psi_{s\alpha\beta}^*[k]=\left|\psi_s[k]\right|^* e^{j\theta_s^*[k]} \quad (42)$$

In which, the desirable stator flux vector is obtained from equation (41), and its magnitude from Maximum

Torque per Ampere (MTPA) strategy [28, 29].

By taking into account the effect of stator resistance, the desired stator voltage vector is written in the discrete time domain as:

$$u_{s\alpha\beta}[k]=\frac{\psi^{*}_{s\alpha\beta}[k]-\psi_{s\alpha\beta}[k]}{T_s}+R_s i_{s\alpha\beta}[k] \qquad (43)$$

The complete scheme of discrete time control for the direct drive PMSG is shown in Fig. 3. According to Fig. 3, in this method, the purpose is to calculate the stator voltage vector command. According to Fig. 4, a reference flux vector estimator (RFVE) is used to calculate the desired stator flux vector by using the information of estimated and reference values of the stator flux and active power and without PI controllers in its structure. Then, a comparison of the stator flux vector to its reference value yields the stator voltage vector command. Then, the proper switching signal is obtained by the SVM.

The stator flux is obtained as:

$$\psi_s=\int(V_s-R_s i_s)dt \qquad (44)$$

The problem, however, is that pure integration suffers from saturation problems due to the initial conditions and DC offset and the effect of drift. To overcome such problems in the whole range of speeds, the low pass filter (LPF) presented in [25] can be used instead. The cutoff frequency of LPF (ω_c) is adjusted proportionally to the rotor electric speed i.e. (ω_c = kω_e). The general scheme of LPF used for the stator flux estimation in discrete time domain is shown in Fig. 5.

The time derivative part is represented by the backward Euler differentiation as:

$$S=\left(1-Z^{-1}\right)/T_s \qquad (45)$$

where T_s is the sampling period.

The stator fluxes after compensation have the form of:

$$\psi_{s\alpha}=g_c\left(\psi'_{s\alpha}\times\cos\theta_c-\psi'_{s\beta}\times\sin\theta_c\right) \qquad (46)$$

$$\psi_{s\beta}=g_c\left(\psi'_{s\alpha}\times\sin\theta_c-\psi'_{s\beta}\times\cos\theta_c\right) \qquad (47)$$

where $\psi'_{s\alpha\beta}$ is the stator flux estimation before compensation.

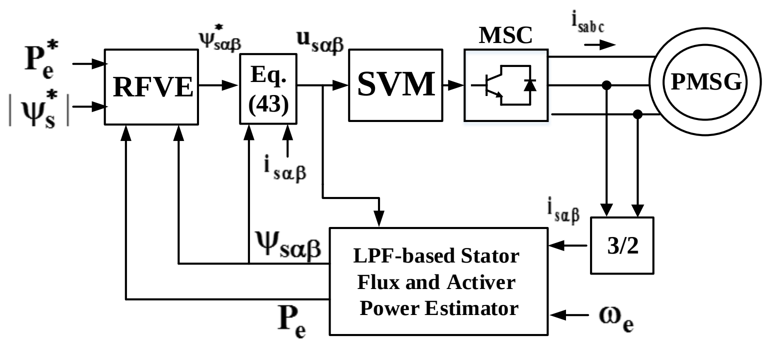

Fig. 3 Proposed schematic for direct-drive PMSG wind turbine.

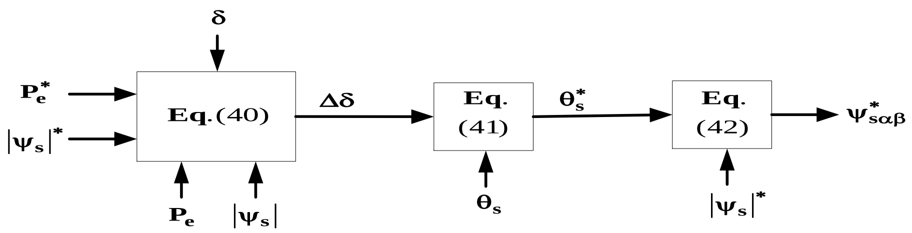

Fig. 4 Block diagram of RFVE.

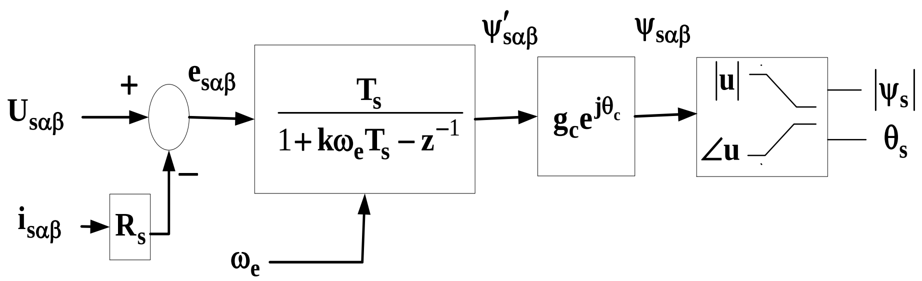

Fig. 5 LPF based on stator flux estimate in the discrete time state.

The gain compensator g_c and phase compensator θ_c for the output of LPF are defined as follows:

$$g_c = \sqrt{(1+k^2)} \tag{48}$$

$$\theta_c = \frac{\pi}{2} - \tan^{-1}\left(\frac{1}{k}\right) \tag{49}$$

4 Simulation Results

Simulations are performed with MATLAB/Simulink software. To demonstrate the validity of the proposed control scheme, its results are compared with the result of the vector control method optimized by the PSO algorithm. The block diagram of the vector control method is shown in Fig. 6. The considered generators are a 1.5MW SPMSG and a 3MW IPMSG. Specifications of the turbine and the generator are listed in Table 1.

The proposed direct control scheme is implemented to discretely control of active power and stator flux of a PMSG-based wind turbine subject to variable wind speed conditions along with MPPT. Afterward, the dependency of the proposed method on the machine parameters is studied and compared with the vector control method with optimized PI coefficients.

4.1 Active Power and Stator Flux Control under Variable Wind Speed Conditions

The same wind speed profile is considered for both the proposed and vector control methods. The wind speed changes in three steps for SPMSG and IPMSG according to Figs. 7(a) and 8(a), respectively.

MPPT is followed by both methods. According to

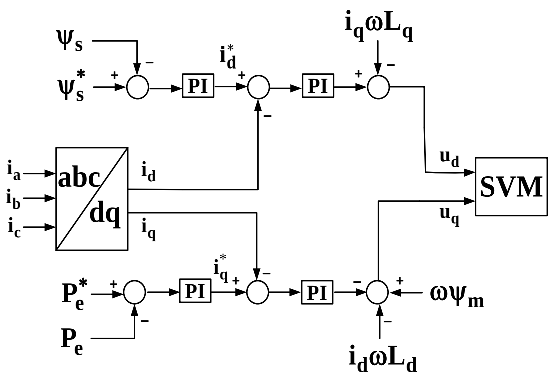

Fig. 6 Block control of vector control method.

Table 1 Specifications of studied turbine and generator [13, 26, 27].

	IPMSG	SPMSG
Nominal power of turbine	3 MW	1.5 MW
Blades radius	45 m	37 m
Air density	1.225 kg/m^3	1.225 kg/m^3
System inertia moment	14.5×10^6 kg.m^2	4.6×10^5 kg.m^2
DC link voltage	6000 v	2000 v
Sampling period	100 µs	100 µs
Nominal power of generator	3 MW	1.5 MW
Number of pole pairs	80	45
Magnet flux linkage	16.2 Wb	7.8 Wb
d-axis inductance	4 mH	3.1 mH
q-axis inductance	6 mH	3.1 mH
Stator resistance	50 mΩ	3.2 mΩ

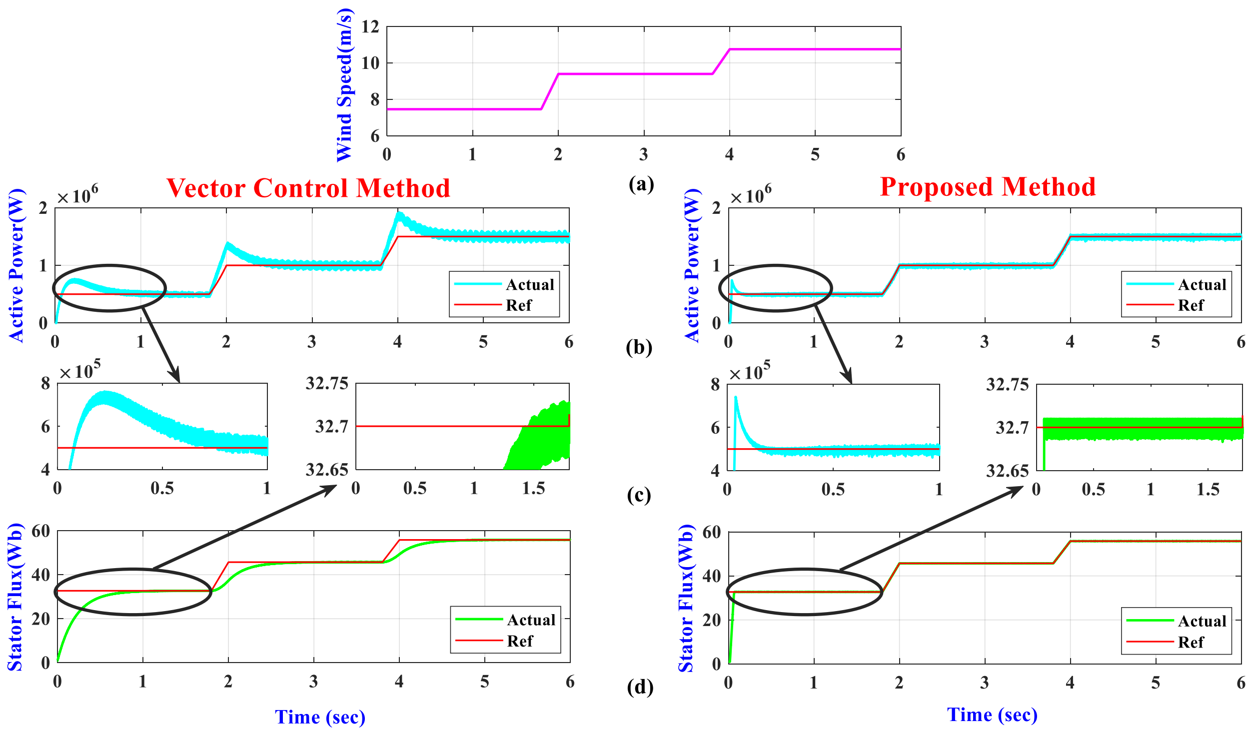

Fig. 7 Active power and stator flux control with two methods for SPMSG; a) wind speed, b) active power, c) zoomed view of active power and stator flux response; d) stator flux [30].

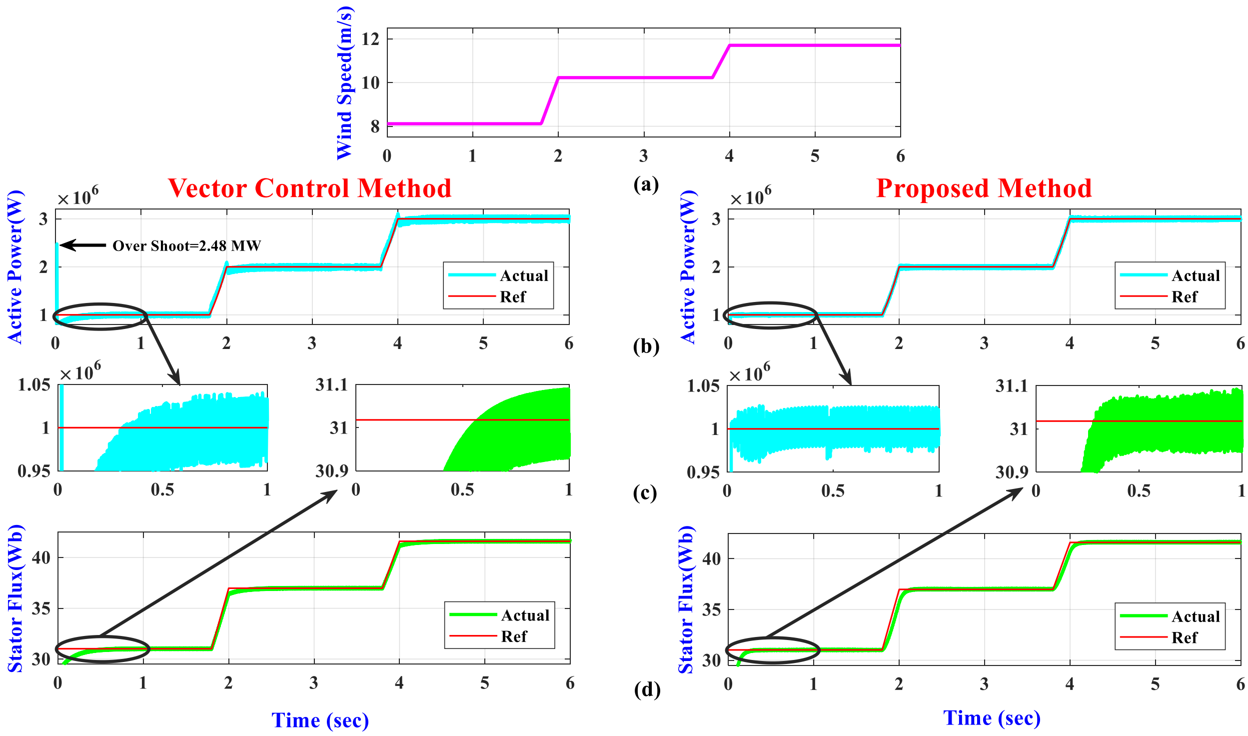

Fig. 8 Active power and stator flux control with two methods for IPMSG; a) wind speed, b) active power, c) zoomed view of active power and stator flux response; d) stator flux.

Table 2 Specifications of the dynamic response of vector and proposed control methods for SPMSG

	Active power response			Stator flux response		
	Average ripple [MW]	Settling time [s]	Overshoot [MW]	Average ripple [MW]	Settling time [s]	Overshoot [MW]
Vector control method	0.132	0.78	0.76	0.0796	1.45	0
Proposed control method	0.075	0.155	0.74	0.03	0.066	0

Table 3 Specifications of the dynamic response of vector and proposed control methods for IPMSG

	Active power response			Stator flux response		
	Average ripple [MW]	Settling time [s]	Overshoot [MW]	Average ripple [MW]	Settling time [s]	Overshoot [MW]
Vector control method	0.105	0.32	2.48	0.157	0.58	0
Proposed control method	0.0645	0.019	0	0.14	0.29	0

the wind speed reference and turbine characteristics, the maximum active power that can be attained from wind energy is considered as the active power reference value. The stator flux reference is calculated for MTPA.

Figs. 7 and 8 demonstrate the active power and stator flux control with variable wind speed and with both the methods for SPMSG and IPMSG, respectively. As shown, the active power and stator flux are properly controlled by the vector control and the proposed methods at different wind speeds.

The active power and stator flux response obtained by the optimized vector control method and the proposed control method are compared in terms of the average ripple, the settling time, and the overshoot. The comparisons are given for SPMSG and IPMSG in Tables 2 and 3, respectively.

It can be concluded from the aforementioned figures and tables that the proposed method controls the active power and stator flux of both SPMSG and IPMSG better than the vector control method at different wind speeds. Superior dynamic response and lower average ripple of active power and stator flux are achieved by the proposed method in comparison with the vector control one due to elimination of inner current control loops and no need to coordinate system transformation blocks as well as the PI controllers and their adjustment.

In addition to active power and stator flux response, dynamic response of the turbine shaft speed and turbine power coefficient by the proposed method for both SPMSG and IPMSG-based wind turbines are shown in Fig. 9. The wind speed is assumed as in Figs. 7 and 8. As observed, the turbine shaft speed changes in such a way that the maximum power is captured from the wind. In this case, the power coefficient tracks the

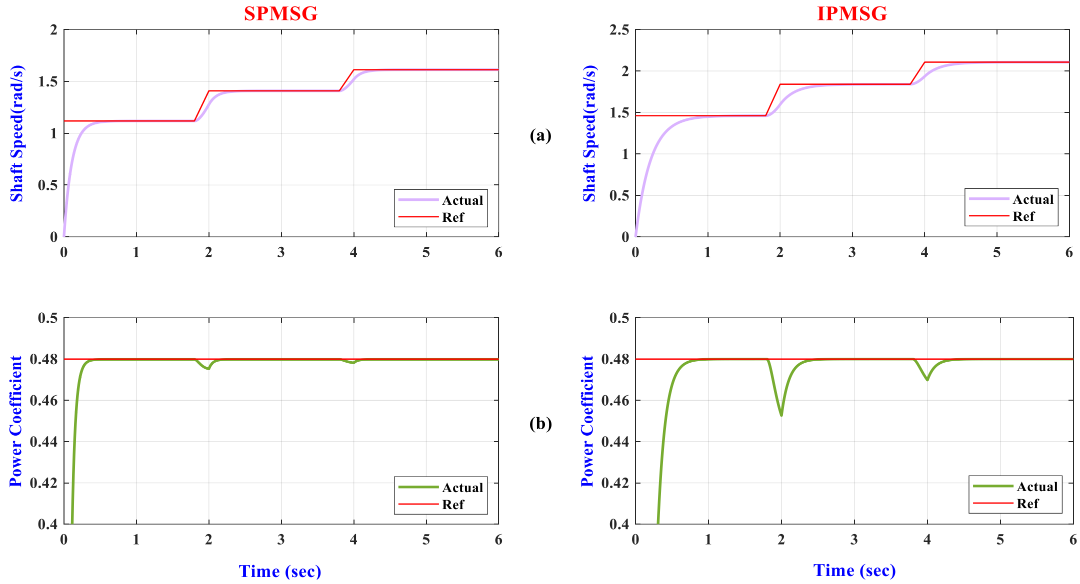

Fig. 9 Dynamic response with the proposed method; a) shaft speed and b) turbine power coefficient.

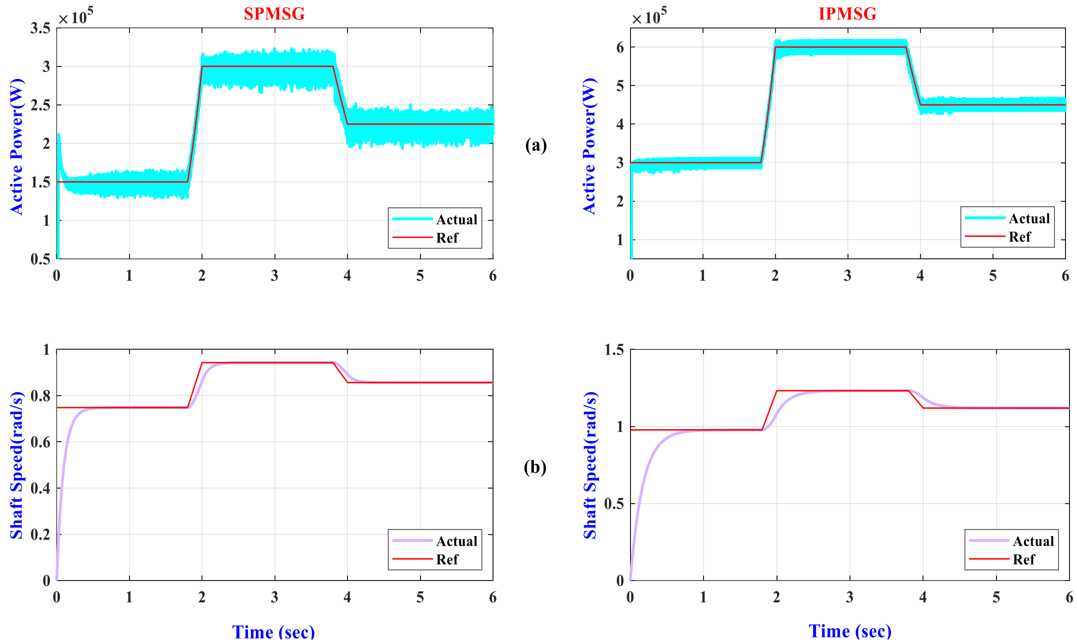

Fig. 10 Operation of the proposed method at light load; a) active power and b) shaft speed.

optimal value of 0.48.

In order to research of proposed method operation at low powers (10% of rated power), simulation is repeated for both SPMSG and IPMSG in Fig. 10. Simulation results are validated higher dynamic response with MPPT achievement for the proposed method. Stator current and voltage at low powers is also shown for the proposed Method and vector control method in Fig. 11.

4.2 Sensitivity Analysis

Sensitivity of the vector and proposed control methods on the machine parameters for IPMSG-based wind turbine are demonstrated in Figs. 12 and 13, respectively. The active power reference is considered to be 1MW for both the methods. In the base case, the machine parameters are fixed to their actual values. As evident from Fig. 12, the active power error in the vector control method increases by approximately 20% with a 10% decrease/increase in the rotor flux value. Furthermore, a 20% decrease and a 20% increase in the stator inductance leads to approximately 60% and 40% error in the active power, respectively. Comparing the sensitivity analysis in Figs. 12 and 13 shows that in the vector control method, it is required to adjust and optimize the PI coefficients again, when the parameters are changed. However, in the proposed method, since the rotor flux and stator inductance are not included in the equations, it is expected that the dependency of the controlling method on the changing of such parameters is reduced. On the other hand, unlike the vector control method, which requires adjusting four PI controllers once again, the proposed method according to (42), with changing the parameters, $\psi^*_{s\alpha\beta}[k]$ is changed as well. According to Figs. 12, the proposed method has negligible sensitivity to the variations in the machine parameters and the changes of parameters does not affect the performance of the controlling method significantly.

5 Conclusions

A novel direct control method for a PMSG-based wind turbine is proposed in this paper, where the active power and stator flux are directly controlled in discrete time domain. This method is applicable to both the SPMSG and IPMSG. The proposed method does not require any inner current control loop and coordinate

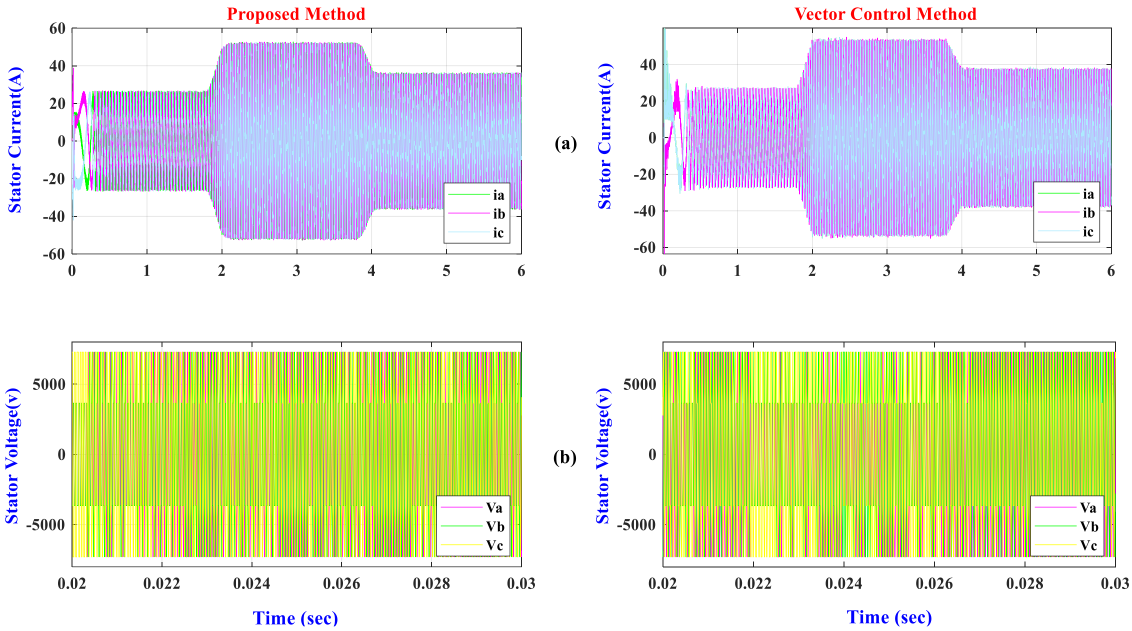

Fig. 11 Stator voltage and current for both methods.

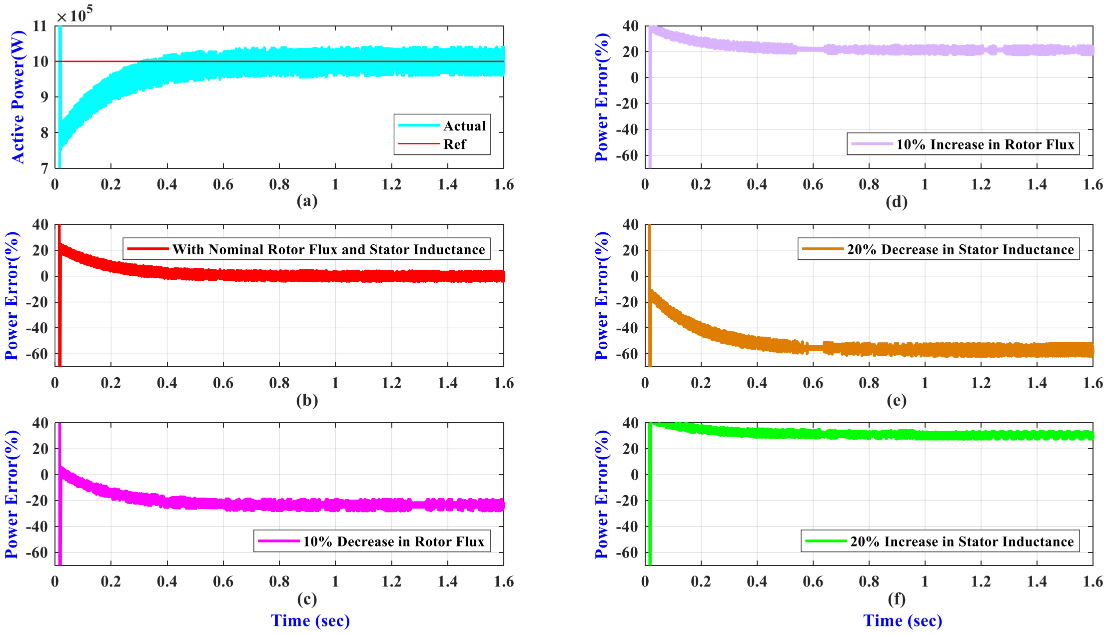

Fig. 12 Influences of variations of machine parameters with the vector control method; a) active power, b) active power error percentage with actual parameters, c) with 10% decrease of rotor flux, d) 10% increase of rotor flux, e) with 20% reduction of stator inductance, and f) with 20% increase of stator inductance.

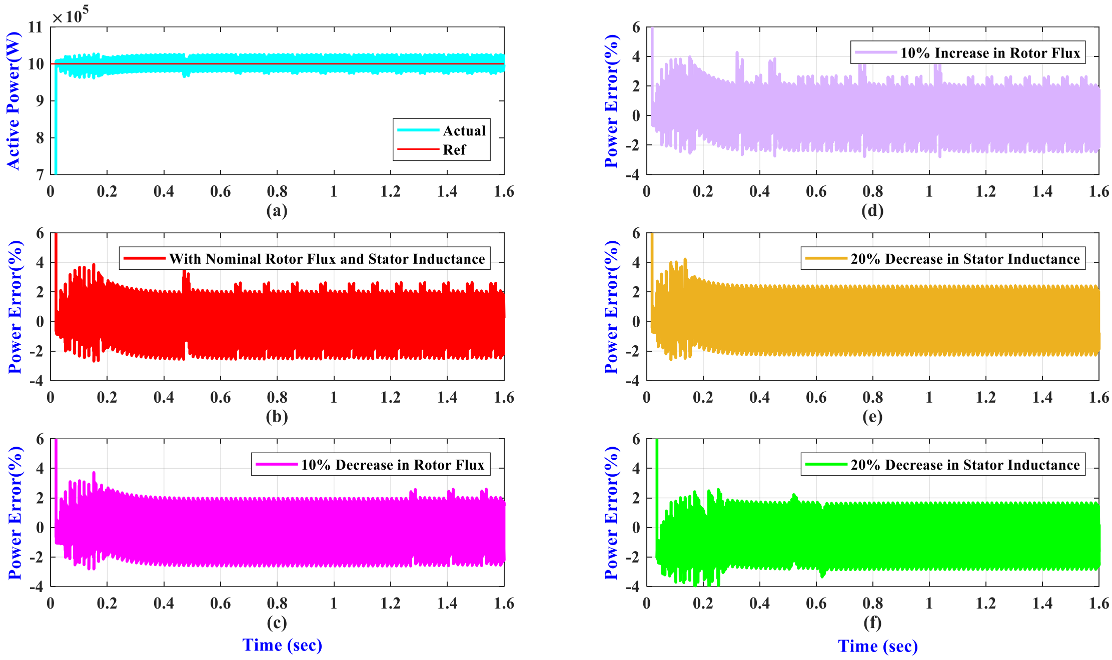

Fig. 13 Influences of variations of machine parameters with the proposed control method; a) active power, b) active power error percentage with actual parameters, c) with 10% decrease of rotor flux, d) with 10% increase of rotor flux, e) with 20% reduction of stator inductance, and f) with 20% increase of stator inductance.

system transformations. According to the time-domain simulations, the proposed method has a higher dynamic response than the vector control method with optimized PI coefficients by the PSO algorithm. In addition, compared to vector control, the proposed method obtains lower error between the reference and actual values of active power and stator flux ripple and overshoot. Furthermore, the proposed control method less depends on the machine parameters which simply shows higher robustness of the system.

References

[1] S. Li, T. A. Haskew, R. P. Swatloski, and W. Gathings, "Optimal and direct-current vector control of direct-driven PMSG wind turbines," *IEEE Transaction on Power Electronics*, Vol. 27, No. 5, pp. 2325–2337, May 2012.

[2] S. M. Tripathi, A. N. Tiwari, and D. Singh, "Optimum design of proportional-integral controllers in grid-integrated PMSG-based wind energy conversion system," *International Transactions on Electrical Energy Systems*, Vol. 26, No. 5, Aug. 2015.

[3] X. Fu and S. Li, "A novel neural network vector control technique for induction motor drive," *IEEE Transactions on Energy Conversion*, Vol. 30, No. 4, pp. 1428–1437, Jun. 2015.

[4] M. A. S. Khan and M. A. Rahman, "A novel nuero-wavelet-based self-tuned wavelet controller for IPM motor drives," *IEEE Transaction on Industry Applications*, Vol. 46, No. 3, pp. 1194–1203, May/Jun. 2010.

[5] N. D. Dao, D. Lee, and S. Lee, "A simple and robust sensorless control based on stator current vector for PMSG wind power systems," *IEEE Access*, Vol. 7, pp. 8070–8080, Dec. 2019.

[6] Y. Abdel and R. I. Mohamed, "Direct instantaneous torque control in direct drive permanent magnet synchronous motor–A new approach," *IEEE Transactions on Energy Conversion*, Vol. 22, No. 4, pp. 829–838, Dec. 2007.

[7] H. Ziane, J. M. Retife, and T. Rekioua, "Fixed-switching-frequency DTC control for PM synchronous machine with minimum torque ripple," *Canadian Journal of Electrical and Computer Engineering*, Vol. 33, No. 34, pp. 183–189, Dec. 2008.

[8] Y. Zhang and J. Zhu, "Direct torque control of permanent magnet synchronous motor with reduced torque ripple and commutation frequency," *IEEE Transactions on Power Electronics*, Vol. 26, No. 1, pp. 235–248, Jan. 2011.

[9] Z. Wang, J. Chen, M. Cheng, and K. T. Chau, "Field-oriented control and direct torque control for paralleled VSIs fed PMSM drives with variable switching frequencies," *IEEE Transactions on Power Electronics*, Vol. 31, No. 3, pp. 2417–2428, Mar. 2016.

[10] X. Wang, Z. Wang, and Z. Xu, "A hybrid direct torque control scheme for dual three-phase PMSM drives with improved operation performance," *IEEE Transactions on Power Electronics*, Vol. 34, No. 2, pp. 1622–1634, Feb. 2019.

[11] Z. Huaqiang, W. Xinsheng, and W. Pengfei, "Study on direct torque control algorithm based on space vector modulation," *Electric Machines and Control*, Vol. 16, No. 6, pp. 13–18, 2012.

[12] C. Lascu, I. Boldea, and F. Blaabjerg, "A modified direct torque control for induction motor sensorless drive," *IEEE Transaction on Industrial Applications*, Vol. 31, No. 1, pp. 122–130, Jan./Feb. 2000.

[13] Z. Zhang, Y. Zhao, W. Qiao, and L. Qu, "A space-vector modulated sensorless direct-torque control for direct-drive PMSG wind turbines," *IEEE Transaction on Industrial Applications*, Vol. 50, No. 4, pp. 2331–2341, 2014.

[14] M. H. Vafaie, B. M. Dehkordi, P. Moallem, and A. Kiyoumarsi, "Minimizing torque and flux ripples and improving dynamic response of PMSM using a voltage vector with optimal parameters," *IEEE Transactions on Industrial Electronics*, Vol. 63, No. 6, pp. 3876–3888, Jun. 2016.

[15] Z. Zhang and R. Kennel, "Novel ripple reduced direct model predictive control of three-level NPC active front end with reduced computational effort," in *IEEE International Symposium on Predictive Control of Electrical Drives and Power Electronics (PRECEDE)*, Valparaiso, Chile, pp. 32–37, Oct. 2015.

[16] S. Vazquez, A. Marquez, R. Aguilera, D. Quevedo, J. Leon, and L. Franquelo, "Predictive optimal switching sequence direct power control for grid-connected power converters," *IEEE Transactions on Industrial Electronics*, Vol. 62, No. 4, pp. 2010–2020, Apr. 2015.

[17] H. Fang, Z. Zhang, X. Feng, and R. Kennel, "Ripple-reduced MPDPC for active front end power converters with extended switching vectors and time-optimized control," *IET Power Electronics*, Vol. 9, No. 9, pp. 1914–1923, Jul. 2016.

[18] Y. Zhang, W. Xie, Z. Li, and Y. Zhang, "Model predictive direct power control of a PWM rectifier with duty cycle optimization," *IEEE Transactions on Power Electronics*, Vol. 28, No. 11, pp. 5343–5351, Nov. 2013.

[19] M. Pacas and J. Weber, "Predictive direct torque control for the PM synchronous machine," *IEEE Transactions on Industrial Electronics*, Vol. 52, No. 5, pp. 1350–1356, Oct. 2005.

[20] I. Boldea, M. C. Paicu, G. D. Andreescu, and F. Blaabjerg, "Active flux DTFC-SVM sensorless control of IPMSM," *IEEE Transaction on Energy Conversion*, Vol. 24, No. 2, pp. 314–322, Jun. 2009.

[21] I. Boldea, M. C. Paicu M. C, and G. D. Andreescu, "Active flux concept for motion-sensorless unified AC drives," *IEEE Transactions On Power Electronics*, Vol. 23, No. 5, pp. 2612–2618, Sep. 2008.

[22] P. Vas, *Sensorless vector and direct torque control*. Oxford University Press, 1998.

[23] C. Lai C, G. Feng, K. Mukherjee, C. and Kar, "Investigations of the influence of PMSM parameter variations in optimal stator current design for torque ripple minimization," *IEEE Transactions on Energy Conversion*, Vol. 32, No. 3, pp. 1052–1062, Mar. 2017.

[24] A. M. Aljehaimi and P. Pillay, "Novel flux linkage estimation algorithm for a variable flux PMSM," *IEEE Transactions on Industrial Electronics*, Vol. 54, No. 3, pp. 2319–2335, Jan. 2018.

[25] M. Shin, D. Hyun, S. Cho, and S. Choe, "An improved stator flux estimation for speed sensorless stator flux orientation control of induction motors," *IEEE Transactions on Power Electronics*, Vol. 15, No. 2, pp. 312–318, Mar. 2000.

[26] M. Kuschke and K. Strunz, "Energy-efficient dynamic drive control for wind power conversion with PMSG: Modeling and application of transfer function analysis," *IEEE Journal of Emerging and Selected Topics in Power Electronics*, Vol. 2, No. 1, pp. 35–45, Mar. 2014.

[27] C. Huang, F. Li, and Z. Jin, "Maximum power point tracking strategy for large-scale wind generation systems considering wind turbine dynamics," *IEEE Transactions on Industrial Electronics*, Vol. 54, No. 3, pp. 2319–2335, Jan. 2015.

[28] T. Inoue, Y. Inoue, S. Morimoto, and M. Sanada, "Maximum torque per ampere control of a direct torque-controlled PMSM in a stator flux linkage synchronous frame," *IEEE Transactions on Industry Applications*, Vol. 52, No. 3, pp. 2360–2367, May/Jun. 2016.

[29] A. Shinohara, Y. Inoue, S. Morimoto, and M. Sanada, "Direct calculation method of reference flux linkage for maximum torque per ampere control in DTC-based IPMSM drives," *IEEE Transactions on Power Electronics*, Vol. 32, No. 3, pp. 2114–2122, Mar. 2017.

[30] S. Tohidi, B. Mamipour Matanag, and N. Rostami, "A new method for direct and discrete control of the PMSG in a wind turbine without need to coordinate transform," *Tabriz Journal Of Electrical Engineering*, Vol. 49, No. 2, pp. 539–550, 2019.

B. Mamipour Matanag was born in Tabriz, Iran, in 1986. He received M.Sc. degree from the University of Tabriz, Iran. He is proficient in programming and simulation with MATLAB software. His research interests include electric machines and drives, and wind power generation.

N. Rostami was born in Ahar, Iran, in 1984. He received the B.Sc. degree from the Khajeh Nasir Toosi University of Technology, Tehran, Iran, in 2006, the M.Sc. degree from the University of Tehran, Tehran, in 2008, and the Ph.D. degree from the University of Tabriz, Tabriz, Iran, in 2013, all in Electrical Engineering. He is currently an Assistant Professor with the Department of Electrical Engineering, University of Tabriz. He is involved in the electric machines branch. He is proficient in finite-element software. His current research interests include electric machines and drives, and electric and hybrid vehicles.

S. Tohidi was born in Meshkin Shahr, Iran, in 1984. He received the B.Sc. degree from Iran, University of Science and Technology (IUST), Tehran, Iran, in 2006, and M.Sc. degree from Sharif University of Technology, Tehran, Iran, in 2008, both in Electrical Engineering. He is currently an Associate Professor at the University of Tabriz, Iran. His research interests include power systems dynamics, electrical machines, and wind power generation.